Quantifying the linear damping in two-dimensional turbulence

Jin-Han Xie[*]
Department of Mechanics and Engineering Science at College of Engineering, LTCS and BIC-ESAT, Peking University, Beijing 100871, People's Republic of China

(Received 14 April 2020; accepted 9 September 2020; published 29 September 2020)

Linear damping is widely applied in experiments and fluid models to describe the large-scale dissipation that absorbs upscale energy transfers in two-dimensional (2D) turbulence. However, in many systems, it is not justified that linear damping is a good model and it is hard to obtain the damping coefficient from directly measurable quantities. Based on the forcing-scale resolving structure-function theory of homogeneous isotropic 2D turbulence derived by Xie and Bühler [J. Fluid Mech. **851**, 672 (2018)], we propose a procedure that simultaneously obtains the magnitude of energy flux, the energy injection scale, and the damping coefficient by fitting the measurable second- and third-order velocity structure functions. Also, a test function based on the structure-function theory is proposed to justify the form of linear damping on each scale. The validity of this procedure is tested against data obtained from numerical simulations.

DOI: 10.1103/PhysRevFluids.5.094605

I. INTRODUCTION

Two-dimensional (2D) turbulence, which even though never realized in nature, has been studied as a prototype that is closely relevant to physical systems such as the large-scale motions of the atmospheric and oceanic flows (cf. Ref. [1]), thin-film flow (e.g., Ref. [2]) and bacteria-involved flows (e.g., Ref. [3]). Under the assumption of homogeneity and isotropy, opposite to the three-dimensional (3D) turbulence [4], energy is found to transfer upscales in 2D turbulence in an infinitely large domain, accompanying with a downscale enstrophy transfer [5,6]. In the energy inertial range, the energy spectrum follows the "5/3-law", $E(k) \sim k^{-5/3}$, while in the enstrophy inertial range, the energy spectrum behaves like $E(k) \sim k^{-3}$ with a log-correction [7].

Same as the Kolmogorov [4]'s structure-function theory for 3D homogeneous isotropic turbulence, relations linking the third-order structure functions with the energy and enstrophy fluxes are obtained in the energy and enstrophy inertial ranges, respectively, for 2D turbulence [8–10]. The Kolmogorov-like theories are one of a few exact results that are obtained directly from the Navier-Stokes equation, and they are essential for both theoretical study and data analyzing. Recently, Xie and Bühler [11] obtained a universal expression for the third-order structure function of 2D turbulence that expresses the two inertial-range results in one formula and the transition between the two inertial ranges, the forcing scale, is also captured. The ability to capture the region away from the classic inertial ranges makes this theory practically useful.

Because energy transfers upscale in 2D turbulence, to reach a statistically steady state, a large-scale damping is required. The linear damping is widely used in numerical simulations (cf. Ref. [12]), and it is used to model the damping effect due to the surrounding environment on fluid systems, such as geophysical flows [13], thin-layer flow [14,15], and soap-film flow [16].

[*]jinhanxie@pku.edu

The large-scale damping is expected to influence the large-scale flow. Smith and Yakhot [17] find that when there is no large-scale damping, energy condensates at large scale in a finite-size 2D turbulence, and, finally, the energy accumulation stops due to the viscosity (cf. Ref. [18]). The steady states of condensation can be vortices or jets, when weak large-scale damping presents, Falkovich [19] find that the condensation states change depending on the domain geometry and the damping form. Particularly, in the limit of weak forcing and dissipation, Bouchet *et al.* [20] apply a quasilinear approach to calculate the shape of the large-scale condensation.

Linear damping also brings about a leading order influence to the enstrophy inertial range. Contrast to the dimensional analysis, linear damping drives the energy spectrum in the enstrophy inertial range to the scaling $E(k) \sim k^{-3+\xi}$ with $\xi > 0$ (cf. Ref. [1]). Nam *et al.* [21] explain the extra exponent ξ as a result of the advection of small scales by large-scale strain, based on which the relation between ξ and the damping coefficient is obtained.

In natural systems, e.g., geophysical flow, and experimental setups such as thin-layer flow, we may argue that the large-scale dissipation can be modelled by a linear damping based on the theories of laminar flow. When the flow is turbulent, by assuming the form of linear damping we may calculate the damping coefficient from the decay rate of the energy density in a free-decay experiment; however, there is no existing theory justifying the validity of linear damping. So we need a method which can use measurable quantities in a 2D turbulent flow to justify the form of linear damping and to obtain the value of damping coefficient. The structure-function theory is well suited for this target. The formulation in Ref. [11] implies that the dissipation effect can be contained in an expression that links the second- and third-order structure functions, energy flux and the forcing scale, which initiates this paper. The power of the structure-function theory is the ability to justify the linear-damping form at each scale which is impossible from a global quantity estimation.

Because condensation brings about inhomogeneity and anisotropy to 2D turbulence, in this paper, to apply the structure-function theories we focus on the case where the linear damping is strong enough that the condensation is suppressed. In Sec. II we show the derivation of the theory for structure functions; then, in Sec. III based on the theory we propose a data analyzing procedure and justify the procedure using data obtained from a controlled numerical simulation. Finally, we summarize and discuss our results in Sec. IV. We provide the details of a numerical simulation with a single forcing scale in Sec. III, and in the Appendix we present a case with two distinctive forcing scales to show the ability of our procedure.

II. STRUCTURE-FUNCTION THEORY FOR TWO-DIMENSIONAL TURBULENCE

We consider forced-dissipative incompressible two-dimensional flow described by the following governing equations:

$$\partial_t \boldsymbol{u} + \boldsymbol{u}\cdot\nabla\boldsymbol{u} = -\nabla p - (-1)^a \alpha \nabla^{-2a}\boldsymbol{u} - (-1)^b \nu \nabla^{2b}\boldsymbol{u} + \boldsymbol{F}, \tag{1a}$$

$$\nabla\cdot\boldsymbol{u} = 0, \tag{1b}$$

where $\boldsymbol{u} = (u,\ v)$ is the 2D velocity vector, the uniform density has been absorbed in the pressure p, and $\boldsymbol{F}$ is a random body force. Here the dissipation terms contain both hyper- and hypoviscosity which are used to model physical processes and are widely applied in numerical simulations. The hypo- and hypoviscosity, α and ν, are both positive and the coefficients a and b are both positive.

The random force $\boldsymbol{F}$ is prescribed to have zero mean and is homogeneous in space and stationary in time. Therefore

$$\overline{\boldsymbol{F}(\boldsymbol{x},t)} = 0 \quad \text{and} \quad \overline{\boldsymbol{F}(\boldsymbol{x}_1,t_1)\cdot\boldsymbol{F}(\boldsymbol{x}_2,t_2)} = C(\boldsymbol{x}_2-\boldsymbol{x}_1, t_2-t_1), \tag{2}$$

with the covariance function C. Here the overbar denotes a statistical averaging, and $\boldsymbol{x}_i$ and t_i ($i = 1, 2$) denote two locations and time.

The random force and the governing equations (1) imply that the turbulent flow has a zero mean, i.e., $\overline{\boldsymbol{u}} = 0$, and is spatially homogeneous. Therefore the covariance

$$\overline{\boldsymbol{u}(\boldsymbol{x}_1, t) \cdot \boldsymbol{u}(\boldsymbol{x}_2, t)} = \overline{\boldsymbol{u}_1 \cdot \boldsymbol{u}_2} \tag{3}$$

depends only on the displacement vector $\boldsymbol{x} = \boldsymbol{x}_2 - \boldsymbol{x}_1$. Homogeneity also implies that the spatial derivatives with respect to the different spatial variables, $\boldsymbol{x}$, $\boldsymbol{x}_1$, and $\boldsymbol{x}_2$, obey the following relation:

$$\nabla = -\nabla_1 = \nabla_2. \tag{4}$$

Multiplying $\boldsymbol{u}_1$ with the governing equation (1) evaluated at $\boldsymbol{x}_2$, adding the conjugate equation, and taking ensemble averaging (e.g., Refs. [22,23]) we obtain the Kármán–Howarth-Monin (KHM) equation

$$\tfrac{1}{2}\partial_t(\overline{\boldsymbol{u}_1 \cdot \boldsymbol{u}_2}) - \tfrac{1}{4}\nabla \cdot \boldsymbol{V} = [-(-1)^a \alpha \nabla^{-2a} - (-1)^b \nu \nabla^{2b}]\overline{\boldsymbol{u}_1 \cdot \boldsymbol{u}_2} + P, \tag{5}$$

which is an exact statistical equation with variables that only depend on the displacement vector $\boldsymbol{x}$ and time t. Here the power input term is

$$P(\boldsymbol{x}, t) = \tfrac{1}{2}\left(\overline{\boldsymbol{u}_1 \cdot \boldsymbol{F}_2} + \overline{\boldsymbol{F}_1 \cdot \boldsymbol{u}_2}\right) \tag{6}$$

and

$$P(0, t) = \overline{\boldsymbol{u} \cdot \boldsymbol{F}} = \epsilon \tag{7}$$

defines ϵ as the energy injection rate. The third-order structure function vector $\boldsymbol{V}$ is

$$\boldsymbol{V}(\boldsymbol{x}, t) = \overline{|\delta \boldsymbol{u}|^2\, \delta \boldsymbol{u}} \tag{8}$$

with $\delta \boldsymbol{u} = \boldsymbol{u}_2 - \boldsymbol{u}_1$ the velocity difference between the velocity measured at two points $\boldsymbol{x}_2$ and $\boldsymbol{x}_1$. In the procedure of deriving the KHM equation (5) we have used the incompressibility condition (1b) to to express $\boldsymbol{V}$.

In a statistically steady state, the KHM equation (5) becomes

$$\nabla \cdot \boldsymbol{V} = 4[(-1)^a \alpha \nabla^{-2a} + (-1)^b \nu \nabla^{2b}]\overline{\boldsymbol{u}_1 \cdot \boldsymbol{u}_2} - 4P, \tag{9}$$

which provide us a relation that links the third-order structure function, second-order structure function, and the external energy injection.

Especially, taking the displacement to zero, i.e., $\boldsymbol{x} = \boldsymbol{0}$, the nonlinear term relating to the third-order structure function is zero and the steady KHM equation recovers the total energy balance

$$\alpha|\nabla^{-a}\boldsymbol{u}|^2 + \nu|\nabla^b \boldsymbol{u}|^2 = P(0) = \epsilon. \tag{10}$$

Subtracting (10) from the steady KHM equation (9) we obtain

$$\nabla \cdot \boldsymbol{V} = 4[(-1)^a \alpha \nabla^{-2a} + (-1)^b \nu \nabla^{2b}]\overline{\boldsymbol{u}_1 \cdot \boldsymbol{u}_2} - 4(\alpha|\nabla^{-a}\boldsymbol{u}|^2 + \nu|\nabla^b \boldsymbol{u}|^2) - 4P + 4\epsilon. \tag{11}$$

It is discussed in Ref. [11] that due to the upscale energy transfer in 2D turbulence we need to the subtraction of energy equation in the derivation of the expression of the third-order structure function in the limit of infinite Reynolds number.

Since in the nonlinear term the third-order structure function is a vector, it is not easy to directly use the steady KHM equation (9) alone to obtain the expression for $\boldsymbol{V}$. Under the assumption of isotropy, the statistical vector fields are functions of the distance of the two measured point, $r = |\boldsymbol{x}|$, particularly, for the third-order structure function we obtain

$$\boldsymbol{V} = V(r)\,\hat{r}, \quad \text{where} \quad \hat{\boldsymbol{r}} = \frac{\boldsymbol{x}}{r}. \tag{12}$$

We can express the scalar function V by

$$V = \overline{\delta u_L^3} + \overline{\delta u_L \delta u_T^2}, \tag{13}$$

where $\overline{\delta u_L^3}$ and $\overline{\delta u_L \delta u_T^2}$ are the longitudinal and transversal third-order structure functions, respectively. Here

$$\delta u_L = \delta \boldsymbol{u} \cdot \hat{\boldsymbol{r}} \quad \text{and} \quad \delta u_L = \delta \boldsymbol{u} \cdot \hat{\boldsymbol{n}}, \tag{14}$$

where $\hat{\boldsymbol{n}}$ is an unit vector satisfying $\hat{\boldsymbol{r}} \cdot \hat{\boldsymbol{n}} = 0$. Isotropy and incompressibility also imply the relation

$$\overline{\delta u_L \delta u_T^2} = \frac{r}{3} \frac{d}{dr} \overline{\delta u_L^3}. \tag{15}$$

As to the second-order structure function, we obtain

$$\overline{|\delta \boldsymbol{u}|^2}(r) = \overline{\delta u_L^2} + \overline{\delta u_T^2}. \tag{16}$$

The incompressibility condition implies that

$$\overline{\delta u_T^2} = \frac{d}{dr}\left(r \overline{\delta u_L^2}\right), \tag{17}$$

leading to

$$2\left(\overline{u^2} - \overline{\boldsymbol{u}_1 \cdot \boldsymbol{u}_2}\right) = \overline{|\delta \boldsymbol{u}|^2} = \frac{1}{r} \frac{d}{dr}\left(r^2 \overline{\delta u_L^2}\right) = \nabla \cdot \left(\boldsymbol{r} \overline{\delta u_L^2}\right). \tag{18}$$

Thus, if the large-scale dissipation is a linear damping, i.e., $a = 0$, the steady KHM equation (11) becomes

$$\nabla \cdot \left(\boldsymbol{V} + 2\alpha \boldsymbol{r} \overline{\delta u_L^2}\right) = 4(-1)^b \nu \nabla^{2b} \overline{\boldsymbol{u}_1 \cdot \boldsymbol{u}_2} - 4\nu \left|\nabla^b \boldsymbol{u}\right|^2 - 4P + 4\epsilon, \tag{19}$$

where the effect of linear damping is absorbed in the divergence.

If the external forcing is white-noise in time and centered at wavenumber $|\boldsymbol{k}| = k_f$, we obtain

$$P = \epsilon J_0(k_f r), \tag{20}$$

where J_0 is the Bessel function of the zeroth order.

When focusing on the scale away from the small viscous scale, which can be estimated as $l_\nu = (\nu^3/\epsilon)^{6a-2}$, we may ignore the ν-dependent term in (19), after integrating once we obtain

$$V = -2\alpha r \overline{\delta u_L^2} + 2\epsilon r - \frac{4\epsilon}{k_f} J_1(k_f r). \tag{21}$$

The expression (21) is the theoretical foundation of this paper and it was mentioned but not fully explored in Ref. [11]. This expression is convenient for practical use because it directly links the measurable second- and third-order structure functions with no spatial derivatives, which potentially increase error when applied to measured data. As to the impact of small-scale dissipation, we may also express it as a function of measurable second-order structure function, but due to the unavoidable spatial derivative we prefer not to tackle it directly.

III. DATA ANALYSIS PROCEDURE

To present our procedure of justifying the form of linear damping and detecting the damping coefficient, we run a numerical simulation of 2D turbulence. The numerical simulation uses a Fourier pseudospectral method with 2/3 dealiasing in space, a resolution 512×512 of a doubly periodic domain $[0, 2\pi] \times [0, 2\pi]$, and a fourth-order explicit Runge–Kutta scheme in time, in which the nonlinear terms are treated explicitly and linear terms implicitly using an integrating factor method. We take the forcing wavenumber to be $k_f = 32$. We add a linear damping with $a = 0$ and a hyperviscosity with $b = 3$ to dissipate energy transferred to large and small scales, respectively, and therefore the turbulence system reaches a statistically steady state so we can use our theoretical expression. We take $\alpha = 0.01$ and $\nu = 1e - 13$ such that $l_\nu \approx 150$.

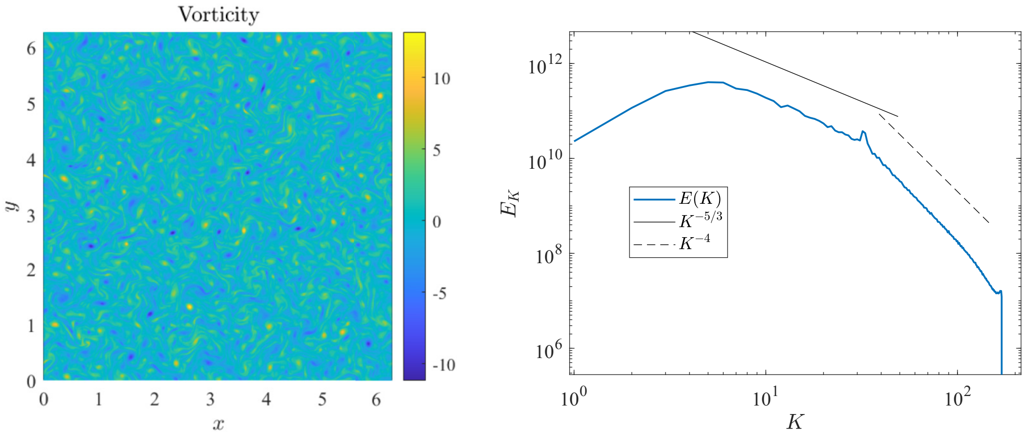

FIG. 1. A snapshot of the vorticity field in the statistically steady state and the energy spectrum.

In Fig. 1 we show a snapshot of the vorticity field in the statistically steady state and the energy spectrum. The energy spectrum shows a Kolmogorov $K^{-5/3}$ spectrum between the large-scale dissipation wavenumber and the forcing wavenumber, corresponding to the energy inertial range, and it shows a K^{-4} spectrum at the enstrophy inertial range. Here the K^{-4} spectrum is steeper than the theoretical K^{-3} prediction may due to the small resolution of the current simulation (cf. Ref. [12]) or the impact of the linear damping [1].

Our theory presented in the previous section is derived under the assumption of isotropy, so we first check the isotropy of third-order structure function using the relation (15). The result is shown in Fig. 2, where we compare the directly measured transversal structure function $\overline{\delta u_L \delta u_T^2}$ against the ones that are reconstructed from the longitudinal third-order structure function using (15). The structure functions measured in both x and y directions are checked. We find that in the region bounded by the two vertical dashed lines the four curves are well coincided, which implies the

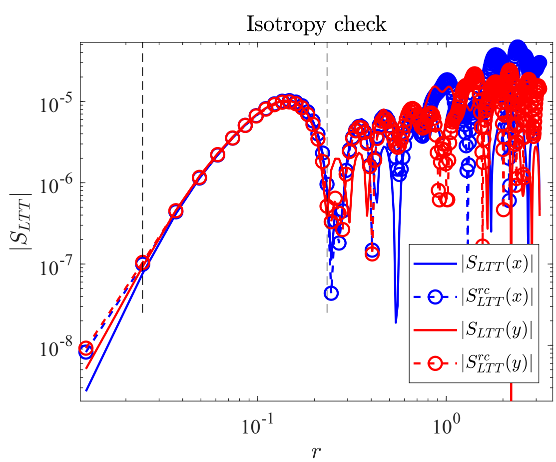

FIG. 2. Isotropy check of the third-order structure functions. The structure functions measured in x and y directions are in blue and red, respectively. The directly measured structure functions and the reconstructed ones are shown in solid and dashed-circle lines, respectively. The two vertical dashed lines indicate the isotropic region bounded in between.

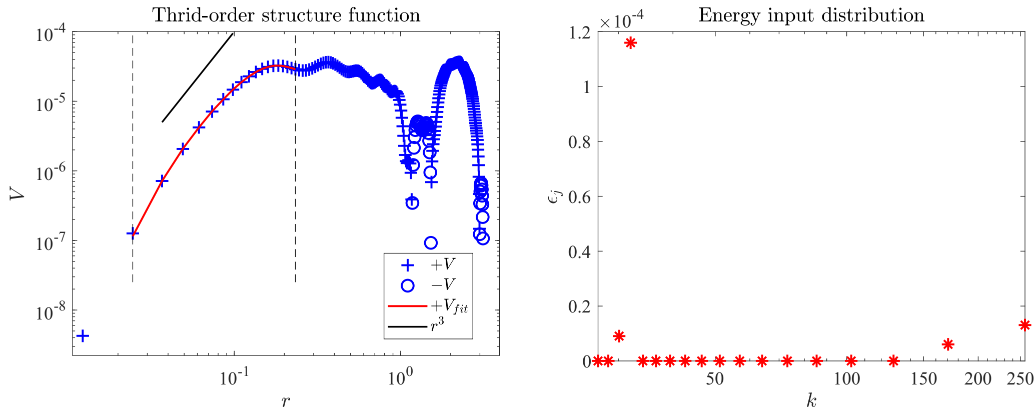

FIG. 3. Curing fitting and detected energy injection. The vertical dashed lines are the same as the one shown in Fig. 2. Here "$+V$" denotes the positive part of the structure function V and "$-V$" means the minus of the structure function when its value is negative. "$+V_{\mathrm{fit}}$" marks the positive part of the fitted structure function. Note that in the present situation, the fitted structure function has no negative part.

isotropy, and therefore we make use of the data in this region to check the form of linear damping and to detect the damping coefficient.

The expression of structure functions (21) is derived based on the assumption that the external forcing is only centered at a single wavenumber k_f. However, in a realistic experiment or measurement we do not know the forcing scale beforehand and the energy injection scale is important information to be detected. Thanks to the linearity of inverse Laplacian in the step of solving (21) from (19), we can expression the structure-function relation with multiple forcing wavenumbers as

$$V = -2\alpha r \overline{\delta u_L \delta u_L} + 2\epsilon r - \sum_{j=1}^{N} \frac{4\epsilon_j}{k_{fj}} J_1(k_{fj} r), \tag{22}$$

where ϵ_j are the energy injections at forcing wavenumber k_{fj}. And for consistency $\epsilon = \sum_{j=1}^{N} \epsilon_j$.

In Fig. 3, we show the least-square fitting of third-order structure function using expression (22) and the detected energy injection rate at different wavenumbers. From numerical data, we obtain the measured distance of two points, the second- and third-order structure functions, and we assume that there is potential energy injection at each forcing wavenumber corresponding to the measured distance $k_f = 2\pi/r$, so the coefficients to be obtained are α, ϵ, and ϵ_j. Due to the isotropy check, we only fit the data in the region bounded by the two vertical dashed lines shown in Fig. 2. The left panel shows a good match between the measured data and the theoretical fitting. From the right panel, we find that our procedure well captures the energy injection scale: The maximum of detected energy injection is at the wavenumber $k = 32$, which is consistent with the prescribed forcing wavenumber. The small nonzero energy injection at large wavenumbers (small scales) are detected due to the error from the influence of small-scale hyperviscosity, which we do not resolve in our expression (22). These artificial energy injections are beyond $k_\nu = 150$, which is consistent with the invalid region of our theoretical result (21).

In Table I, we compare the prescribed coefficients and the ones detected by fitting (22). The prescribed energy injection rate $\epsilon = 1.25 \times 10^{-4}$ is directly calculated because the external forcing is white-noise in time. And, theoretically, $\sum \epsilon_j$ and $\epsilon_j(k_f = 32)$ should have the same value as ϵ. The fitted $\sum \epsilon_j$ is larger than the prescribed value due to the influence of small-scale dissipation, which also brings about an error in detecting the forcing scale: The ϵ_j shown in the right panel of Fig. 3 has small but nonzero values in the neighbor of $k_f = 32$, so the detected $\epsilon_j(k_f = 32)$ is smaller than the prescribed value. The detected ϵ, which corresponds to upscale energy flux (cf.

TABLE I. Comparison of the coefficients prescribed and fitted values in the expression of (22). Here $\epsilon_j(k_f = 32)$ denotes the energy injection rate at wavenumber $k = 32$.

	ϵ	$\sum \epsilon_j$	$\epsilon_j(k_f = 32)$	α
Prescribed	1.25×10^{-4}	1.25×10^{-4}	1.25×10^{-4}	0.01
Fitted	1.19×10^{-4}	1.44×10^{-4}	1.16×10^{-4}	0.0093

Ref. [24]), is close to the prescribed value, which implies that the influence of small-scale dissipation is confined to a local small-scale region in our fitting procedure. Finally, our detected linear damping coefficient matches well the prescribed value with a less than 10% relative error.

We have obtained a value of linear damping coefficient from our expression (22), where the large-scale damping is assumed to be a linear damping. However, this assumption needs to be tested against data at different scales, which shows the power of the structure-function theory. To test the form of linear damping we define the function

$$E = \frac{A(r)}{\alpha_{\mathrm{det}}} - 1, \tag{23}$$

where

$$A(r) = \frac{2\epsilon r - \sum_{j=1}^{N} \frac{4\epsilon_j}{k_{fj}} J_1(k_{fj} r) - V}{2r\overline{\delta u_L^2}}, \tag{24}$$

with V is the measured third-order structure function, and α_{det} is the detected linear-damping coefficient. If the linear damping is a good model, our theory (22) implies that $E(r)$ should be around zero.

The testing function E captures how well the linear damping approximates the damping effect. The relation (22) implies that the third-order structure function V is impacted by three effects: finite-scale effect of linear damping, large-scale energy dissipation, and the energy injection. Here the last two effects are certain, but the first effect is not sure because we want to know if the linear damping is a good form. In the perspective of fitting V, (22) implies that we choose a basis consists of $r\overline{\delta u_L^2}$, r, and $J_1(k_f r)$, and we know that the last two functions are appropriate because these forms are derived from equations for any damping form, but we are not sure if $r\overline{\delta u_L^2}$ is a proper function. Thus, the testing function E describe the relative error brought about by using the linear damping. We plot the function E in Fig. 4, we find that E is close to 0, indicating that linear damping is a proper form. Our theoretical expression (22) is derived by ignoring the small-scale hyperviscosity effect [cf. (19)–(21)], so the magnitude of E decreases as r increases ($<1\%$), i.e., away from the viscous scale l_ν.

Finally, in Fig. 5, we check the robustness of our procedure by varying the end point of the fitting, which may use data in the region that are not obviously isotropic based on the check in Fig. 2. We find that as long as the end point is smaller than $r \approx 1$ the detected α is reasonably good with an error less than 15%. As a comparison, the right vertical dashed line in Fig. 2 is around $r = 0.2$. We find in the left panel of Fig. 3 that $r \approx 1$ corresponds to the sign change of third-order structure function V, which should not exist in an infinite-domain 2D turbulence [11]. The negative V could result from the domain size effect: Since the simulation is taken in a doubly periodic box, when the scale is comparable with the box size, which is 2π in this simulation, isotropy condition cannot hold.

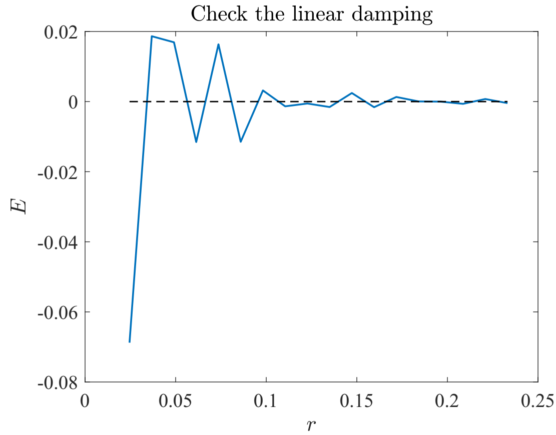

FIG. 4. Checking the form of linear damping using function E. The zero dashed line is plotted as a reference.

IV. SUMMARY AND DISCUSSION

In 2D homogeneous isotropic turbulence, applying the theory for structure functions that captures the inertial range, forcing scale, and linear damping, we propose a procedure that can detect the forcing scale and energy injection, can justify the form of linear damping, and can quantify the damping coefficient. Since the structure-function theory is derived under the assumption of homogeneity and isotropy, the first step of this procedure is to check the isotropy from different components of third-order structure functions measured in different directions; then we can determine the analyzable data range satisfying the isotropy assumption. So in the next step, we fit these analyzable data by the theoretical expression (22) using the least square to obtain the forcing scale, energy injection distribution, and the damping coefficient. Our last step is justifying the damping form by plotting the test function (24) with the fitted coefficients. We tested our procedure in a numerical simulation of 2D turbulence.

Other large-scale damping forms can also absorb upscale energy transfer to saturate the 2D turbulence to statistically steady states, such as the hypoviscosity with $a > 0$, but in this paper, we focus on the case of linear damping, which simplifies the damping resolved theoretical expression

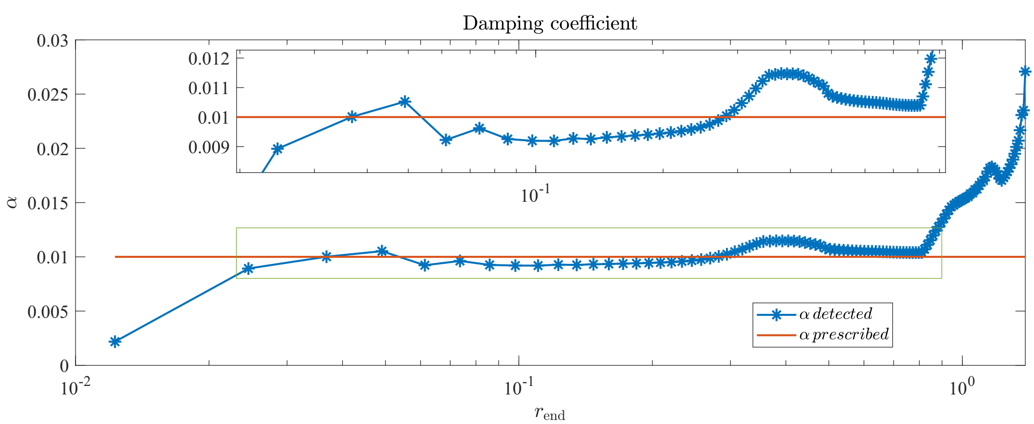

FIG. 5. The dependence of detected linear damping coefficient on the end point of data used for fitting. The horizontal red line denotes the prescribed α. The inset zooms in the rectangle region in the main figure.

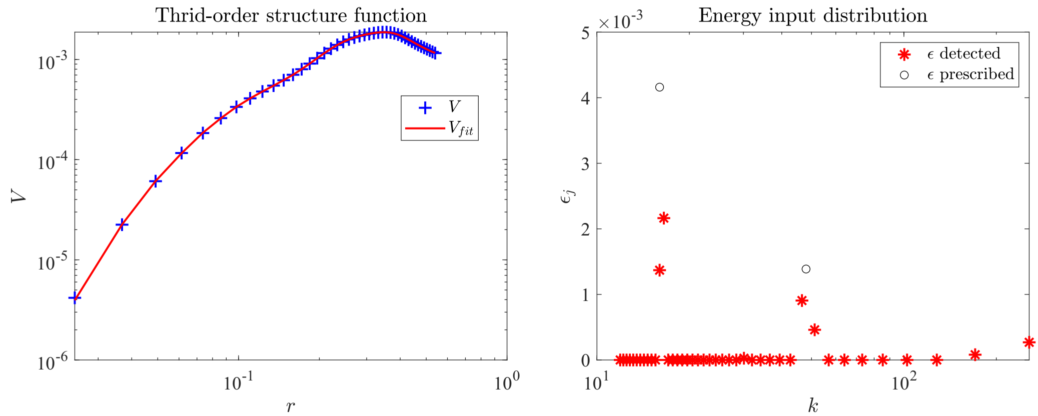

FIG. 6. Curing fitting and detected energy injection. In the right panel the black dots denotes the wavenumber and strength of the prescribed energy injection.

(21) to a form with no spatial derivative. This property is particularly useful for measurements since the spatial derivatives tend to amplify the error of measured data. For the same reason, we do not include small-scale dissipations in our calculation due to their usually associated high spatial derivatives. Also, because the condensation breaks the assumption of homogeneity and isotropy, our method is restricted to the situation where the linear damping is strong enough to prevent the existence of condensation.

In deriving the effect of external forcing, we assumed that the external force is white-noise in time; however, this assumption is not always applicable to the realistic scenarios. So the forcing information detected in our procedure should be understood as an equivalence of a temporal white-noise forcing.

We want to note that even though we focus on the 2D turbulent dynamics, our method should also work for 3D turbulent flows given 2D measurement. For example, the atmospheric and oceanic flows are thought to be governed by rotating stratified turbulence, which shows a combined feature of 2D and 3D turbulence with a simultaneous bidirectional energy transfer to both large and small scales [25]. Since our expression (21) can be generalized to capture bidirectional energy transfer:

$$V = -2\alpha r\overline{\delta u_L^2} + 2\epsilon_u r - \frac{4\epsilon}{k_f}J_1(k_f r), \tag{25}$$

where ϵ_u is the upscale energy transfer magnitude and therefore the downscale energy transfer magnitude is $\epsilon - \epsilon_u$ [26]. So given measured structure function, we could access whether linear damping is an appropriate form for the large-scale damping in the atmospheric and oceanic turbulence.

The assumption of homogeneity and isotropy is the main barrier to applying the present procedure to general situations. To solve this problem several directions are worth exploring, e.g., we can extend the technique of forcing and dissipation resolved structure-function theory to turbulence with shear (cf. Ref. [27]) or when the external forcing has a prescribed anisotropy. For the latter case, we may consider an angle average (cf. Ref. [28]). Another barrier is compressibility. In the Kolmogorov-like theories, the incompressibility is needed to express the nonlinear terms as neat expressions of third-order structure functions, but the structure-function theory for compressible turbulence is much more complicated [29], it is a future direction to study whether we can obtain the information of damping in compressible turbulence.

ACKNOWLEDGMENT

J.-H.X. thanks Yue-Kin Tsang and Ke-Qing Xia for valuable discussions.

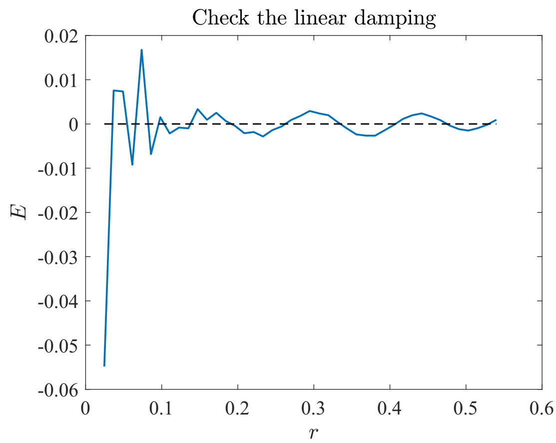

FIG. 7. Checking the form of linear damping using function E. The zero dashed line is plotted as a reference.

APPENDIX: CASE WITH TWO FORCING SCALES

In this section we present the damping coefficient and energy injection detection in a 2D turbulence with external forcing centered around two wavenumbers, $k_{f1} = 16$ and $k_{f2} = 48$, with energy injection rates $\epsilon_1 = 4.2 \times 10^{-3}$ and $\epsilon_2 = 1.4 \times 10^{-3}$, respectively. Because the total injected energy is larger than that applied in the simulation shown in Sec. III, we take the linear-damping coefficient as $\alpha = 0.04$, which is larger than that set in the simulation shown in Sec. III.

In Fig. 6, we show the least-square fitting of third-order structure function using expression (22) and the detected energy injection rate at different wavenumbers. We find that even though our procedure detects a slightly wider energy injection range the energy injection scales are well captured. Also, the detected energy injection around wavenumbers $k_{f1} = 16$ and $k_{f2} = 48$ are $\epsilon_1 = 4.3 \times 10^{-3}$ and $\epsilon_2 = 1.4 \times 10^{-3}$, respectively. This indicates that our procedure well captures the energy injection magnitude.

We justify the form of linear damping in Fig. 7. The detected linear-damping coefficient is $\alpha = 0.0424$, which is within 6% error compared with the prescribed value $\alpha = 0.04$. Similarly to the simulation shown in Sec. III, at small scale the magnitude of E is relatively large due to the impact of small-scale dissipation, and as the scale becomes larger, the magnitude of E decreases (<1%).

[1] G. Boffetta and R. E. Ecke, Two-dimensional turbulence, Annu. Rev. Fluid Mech. **44**, 427 (2011).

[2] R. T. Cerbus and W. I. Goldburg, Intermittency in 2d soap film turbulence, Phys. Fluids **25**, 105111 (2013).

[3] R. T. Cerbus and W. I. Goldburg, Meso-scale turbulence in living fluids, Proc. Natl. Acad. Sci. U.S.A. **109**, 14308 (2012).

[4] A. N. Kolmogorov, Dissipation of energy in locally isotropic turbulence, Dokl. Akad. Nauk SSSR **32**, 16 (1941).

[5] G. K. Batchelor, Small-scale variation of convected quantities like temperature in turbulent fluid. Part 1., J. Fluid Mech. **5**, 113 (1959).

[6] R. H. Kraichnan, Inertial ranges in two-dimensional turbulence, Phys. Fluids **10**, 1417 (1967).

[7] R. H. Kraichnan, Inertial-range transfer in two- and three-dimensional turbulence, J. Fluid Mech. **47**, 525 (1971).

[8] E. Lindborg, Can the atmospheric kinetic energy spectrum be explained by two-dimensional turbulence? J. Fluid Mech. **388**, 259 (1999).

[9] D. Bernard, Three-point velocity correlation functions in two-dimensional forced turbulence, Phys. Rev. E **60**, 6184 (1999).
[10] V. Yakhot, Two-dimensional turbulence in the inverse cascade range, Phys. Rev. E **60**, 5544 (1999).
[11] J.-H. Xie and O. Bühler, Exact third-order structure functions for two-dimensional turbulence, J. Fluid Mech. **851**, 672 (2018).
[12] G. Boffetta and S. Musacchio, Evidence for the double cascade scenario in two-dimensional turbulence, Phys. Rev. E **82**, 016307 (2010).
[13] R. Salmon, *Lectures on Geophysical Fluid Dynamics* (Oxford University Press, Oxford, 1998).
[14] G. Boffetta, A. Cenedese, S. Espa,, and S. Musacchio, Effects of friction on 2d turbulence: An experimental study of the direct cascade, Europhys. Lett. **71**, 590 (2005).
[15] H. Xia, M. Shats, and G. Falkovich, Spectrally condensed turbulence in thin layers, Phys. Fluids **21**, 125101 (2009).
[16] H. Kellay, X.-L. Wu, and W. I. Goldburg, Experiments with Turbulent Soap Films., Phys. Rev. Lett. **74**, 3975 (1995).
[17] S. M. Smith and V. Yakhot, Finite-size effects in forced two-dimensional turbulence, J. Fluid Mech. **274**, 115 (1994).
[18] G. L. Eyink, Exact results on stationary turbulence in 2d: Consequences of vorticity conservation, Physica D **91**, 97 (1996).
[19] G. Falkovich, Interaction between mean flow and turbulence in two dimensions., Proc. R. Soc. A **472**, 20160287 (2016).
[20] F. Bouchet, C. Nardini, and T. Tangarife, Kinetic theory of jet dynamics in the stochastic barotropic and 2d Navier-Stokes equations, J. Stat Phys. **153**, 572 (2013).
[21] K. Nam, E. Ott, T. M. Antonsen, Jr, and P. N. Guzdar, Lagrangian Chaos and the Effect of Drag on the Enstrophy Cascade in Two-Dimensional Turbulence, Phys. Rev. Lett. **84**, 5134 (2000).
[22] A. S. Monin and A. M. Yaglom, *Statistical Fluid Mechanics, Volume II: Mechanics of Turbulence* (Dover, London, 1975).
[23] U. Frisch, *Turbulence: The Legacy of A. N. Kolmogorov* (Cambridge University Press, Cambridge, UK, 1995).
[24] J.-H. Xie and O. Bühler, Third-order structure functions for isotropic turbulence with bidirectional energy transfer, J. Fluid Mech. **877**, R3 (2019).
[25] R. Marino, A. Pouquet, and D. Rosenberg, Resolving the Paradox of Oceanic Large-Scale Balance and Small-Scale Mixing, Phys. Rev. Lett. **114**, 114504 (2015).
[26] J.-H. Xie and O. Bühler, Two-dimensional isotropic inertia–gravity wave turbulence, J. Fluid. Mech. **872**, 752 (2019).
[27] C. M. Casciola, P. Gualtieri, R. Benzi, and R. Piva, Scale-by-scale budget and similarity laws for shear turbulence, J. Fluid Mech. **476**, 105 (2003).
[28] Q. Nie and S. Tanveer, A note on third-order structure functions in turbulence, Proc. R. Soc. Lond. A **455**, 1615 (1999).
[29] S. Banerjee and S. Galtier, A kolmogorov-like exact relation for compressible polytropic turbulence, J. Fluid Mech. **742**, 230 (2014).